

Characterization of Polycrystalline Silicon Substrates (*p*-Type) of Photovoltaic Use

A. LOUNIS*, K. LENOUAR, Y. GRITLY†, B. ABBAD‡ and M. BOUMAOUR†
Laboratory of Sciences and Material Engineering, USTHB, BP32.El Alia, Algiers, Algeria
E-mail: zlounis@yahoo.com

The quality of the material, polycrystalline silicon, is justified by the required features for the final use of the product. It is considered that this quality is due to the impurities which are present in the metal. Carbon, oxygen, boron and transition metals are catalogued among the most frequently observed impurities in silicon, because of their high mobility and solubility in polycrystalline silicon. These impurities generate a yield decrease in the photovoltaic components. The aim of this work is to determine the concentration of impurities such as carbon, iron, copper, titanium, nickel as well as some properties of the flat product such as thickness, resistance, rigidity, roughness and flatness. The dislocations density is also assessed.

Key Words: Multicrystalline silicon, Impurities, Photovoltaic.

INTRODUCTION

In the field of photovoltaic solar energy, polycrystalline silicon is one of the most used materials. The optimization of energy transfer yield remains the everlasting concern of the technologist. In which case can we virtually approach the curves of theoretical yields? It depends on the command of the technological process of material obtaining. The purification and the very high purity are attained by sophisticated techniques, to reach a yield of 20 % whereas at a prohibitive price¹⁻³. The high quality is justified by the required features for the final use of the product. It is considered that this quality is linked to the content of impurities within the metals.

The photo-electronic quality of silicon ingots is limited by the density of dislocations and the recombining role of some grain boundaries⁴. The impurities also reduce very largely the diffusion length of polycrystalline silicon. The grain boundaries activity is also connected to oxygen concentration. The solubility of interstitial copper (Cu_i) in silicon is low and it tends to precipitate at vacancy-like defects, stacking defects, grain boundaries, oxygen precipitates or the sample surface^{5,6}.

†Unit of Silicon Technology Development, UDTS, El-Madania, Algiers, Algeria.

‡Unit of Solar Equipments Development, UDES, Bou Ismail, Algiers, Algeria.

Carbon, oxygen, boron and transition metals are the most commonly observed in silicon because of their high mobility and solubility in polycrystalline silicon. These impurities generate a yield decrease of photovoltaic component⁷⁻⁹.

Geerligs¹⁰ reported that the carbon concentration in most ingots is about 7-11 ppm with relatively flat profiles. Carbon is known to precipitate not easily. Studies of carbon in Czochralski silicon have mainly focused on its enhancement effect on oxygen precipitation¹¹⁻¹⁵ and interactions with silicon self-interstitials (Si_i)^{16,17}. The situation is different in polycrystalline ribbon silicon, which usually contains a high concentration of CS, ranging¹⁸ from 4 to 6.017 cm⁻³.

The material (polycrystalline silicon) used in this study is manufactured by the Unit of Silicon Technology Development (UDTS Algiers, Algeria).

Amid the manufacturing processes, the heat exchanger method (HEM) allows the formation of square sections ingots, starting from a bath of molten silicon.

The aim of this work is to determine the dislocations density, impurities concentration such as oxygen, carbon, iron, copper, titanium, nickel and also some properties of the flat product such as thickness, resistivity, rigidity, roughness and flatness.

For this purpose, the following instrumental analysis techniques have been employed *i.e.*, the inductive sensor, ultrasonic scanner, the resistivity-meter (Valdes method), the infra-red spectroscopy by Fourier's transform (FTIR), the spectrometry of atomic emission, neutronic analysis, electronic scan microscopy, X-rays diffraction and the mass spectrometry.

EXPERIMENTAL

The 80 kg ingot has been cutted into 16 briquettes in order to have plates (flat product) of 100 mm × 100 mm dimensions. The three briquettes, numbered 4, 3 and 6 representative of the ingot, will be the subject of present study.

The first corresponds to the ingot corner, which has two faces in contact with the crucible. The second represents the ingot side, which has only one face in contact with the crucible. The third represents the ingot heart having no face in contact with the crucible. Each briquette is divided into three parts top (T), middle (M) and bottom (B) as indicated in Fig. 1.

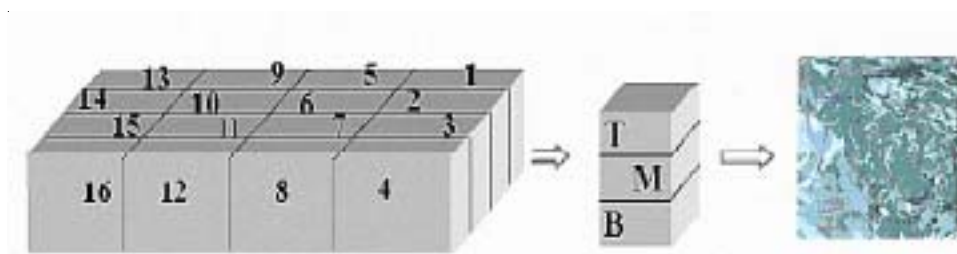


Fig. 1. Selection tablets

From each division, 3 tablets were taken which makes 27 samples to study.

We used an inductive sensor to define the average thickness of the tablets. The sensor measures the thickness with a head related to a magnet under a magnetic field. Five points of measurement are sufficient to have an acceptable result (ASTM).

The measuring sensor is connected to the instrument of digital posting, which transmits the value to a PC. In order to assess the rigidity of our material we were interested in the Young's module. An ultrasonic scanner¹⁹ is used to measure the longitudinal vibrations speed V_λ which depends on the Young's module speed and voluminal mass ρ by relation:

$$V_\lambda = \sqrt{E/\rho} \quad (1)$$

A roughness-meter provided with a (diamond and piezoelectric) crystal informs about the profile and the depths of the current peaks in tablet surface. It is also considered necessary to determine the flatness of these tablets. The resistivity is measured by a 4 points borer^{20,21}. In case of thin layers (300 microns tablets) of depth 'd', the equal-potential is of cylindrical form. We calculated resistance between point 2 and point 3 taking only in consideration the half of the cylindrical crown located in the current flow direction (Fig. 2).

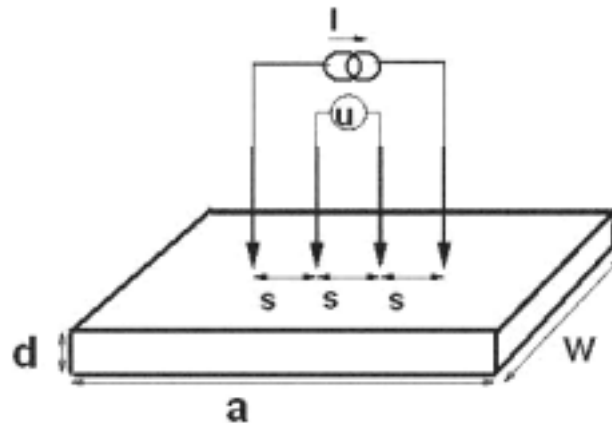


Fig. 2. Resistivity measure

Four points equidistantly aligned are applied by simple pressure on the sample. A current 'I' is injected by the external points using a current source, creating a variation of potential. Thus, a tension 'U' can be measured between two internal points connected to a voltmeter, which is selected with a large impedance interns compared with the one of the sample. It is necessary to introduce a geometrical factor of correction 'C', of which Smith²¹ gives a value table *versus* ratios w/s and a/w , Knowing the thickness 'd' we go back up to the resistivity ' ρ '.

Before carrying out carbon analysis by FTIR and determining resistivity, the samples undergo the following treatment. First used a soda (30 % NaOH) then made a rinsing with distilled water, a washing with hydrochloric acid (HCl 37 %) and a rinsing with deionized water, a second washing with hydrofluoric acid and finally a washing with distilled water in an ultrasonic machine.

The FTIR equipment is Perkin-Elmer type provided with a (GRAMS) software, it allows to have a transmittance *versus* a wave number:

$$(T(\%)) = f(\bar{\nu}) \quad (2)$$

The impurities dosage (Fe, Cu, Ni and Ti) is identified by inductively coupled atomic-plasma emission spectrometry (ICP-AES) Jobin-Ivon type. Several phases are required to set the samples in solution. A very fine crushing of the samples; dissolution in NaOH 100 °C, evaporation to 80 % of the solution, taken again with HNO₃, a wet salt evaporation then proceed to the resumption with distilled water.

The elements detection is accomplished by mass spectroscopy of secondary ion, the secondary ions are created by a very short pulsion of primary ions, bombarding the surface to be analyzed.

For this characterization, the samples marked as 4H, 4M, 4B, 3H, 3M, 3B, 6H, 6M, 6B. To analyze the tablets by SIMS, it is indispensable to cut them into small pieces of 1 cm² (small part of samples). Before sawing the tablets, we immersed them into a resin bath. The samples are plunged in a hot trichloroethylene solution at 85 °C temperature during 5 min, then we rinse them successively in acetone solution in deionized water, finally dried with compressed air.

The nature of the ions determines the characteristics of the analysis. Throughout this analysis we have used according to the cases: (molecular analysis, imaging, profile) a source of caesium ions Cs⁺ 10 keV for the molecular analysis (traces), an isotopic mono source of gallium ions 69 Ga⁺ 15-25 keV for the molecular analysis, imagery and at last an electronic impact source Ar⁺ or O₂⁺ 1-10 keV for the profiles (abrasion gun). Regarding the neutronic analysis activation the irradiations have been realized in the thermal column of the nuclear reactor of Draria -Algiers.

The samples are cleaned as described previously to eliminate the impurities. The lubricant traces and abrasive resulting from the cutting. Masses of 80 mg on average are sampled and form of discs 18 mm in diameter, then exposed to a flux of neutron of 2.10¹² neutron cm⁻² s⁻¹ during 15 min in the thermal column of the nuclear reactor of Draria-Algiers.

The choice of the detection process depends on the transmitter nature and complexity of the emitted spectrum. The most effective solution consists in recording the spectrum γ that comes with the majority of β emissions of the radionuclide present in the samples after activation. The γ spectrum is quantified easily, unlike the β spectrum, continuous in energy.

For the dislocations observation the samples preparation is carried out as follows: After the samples coating, a polishing with abrasive paper, elimination of scratches with a felt, adding a diamond paste in suspension, cleaning with 60° alcohol, the surface quality is controlled using an optical microscope.

The surface attack is obtained by Shimmel solution method based on chromium oxide and hydrofluoric acid. After surface attack the observation under the optical microscope provided with a camera allows the identification of dislocations emergence points^{22,23}. Some methods permit the examination of dislocations emergence points on crystal surface and others provide images of these defects into volume. The statistical observations (surface methods) allows to determine the dislocation density by an optical microscope using a chemical attack which reveals the emergence points of dislocations on the crystal surface²⁴.

According to ASTM (F47-84) standard, nine counting points on the samples can give acceptable results for a routine counting of dislocations as indicated in Fig. 3.

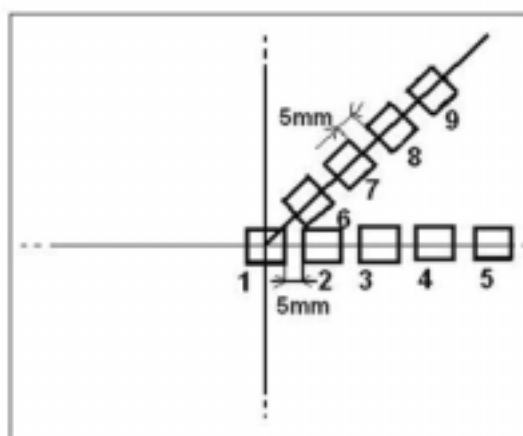


Fig. 3. Counting position for the method according to ASTM (F47-84) standard

Other techniques such as the XRD (X-Ray Diffraction) and Mapping has been applied to give more information for these specimen.

RESULTS AND DISCUSSION

The analysis of results given by inductive sensor displays an average value of tablet thickness of $300 \pm 10 \mu\text{m}$. This value is practically identical to the ones obtained using an electronic micrometer.

The average value of Young's module is 17,71Gpa. Because of the calibration difficulties, this method causes an error of 5 %. In certain points of the samples 19GPa value is obtained. From this it concluded that the materials have an heterogeneity, which proves the existence of certain defects, that are originating from the chemical composition, crystallographic defects, asperities. The maximum value of roughness does not exceed $5.25 \mu\text{m}$. This value is lower than $< 4 \mu\text{m}$.

For other analyzed samples by using a roughness measurement, Perthmeter type S6P, suggests a good surface condition. After calculations, it is found that flatness admits a value equals to 0.0289 mm.

An interval of 0.05mm is sufficient to confirm the tablet flatness or parallelism²⁵.
The expression of resistance for an elementary part is written:

$$dR = \frac{\rho dr}{\pi e r} \quad (3)$$

So:

$$R = \frac{\rho}{\pi e} \int_s^{2s} \frac{dr}{r} \quad (4)$$

integration gives

$$R = \frac{\rho}{\pi e} \text{Ln}2 \quad (5)$$

Or:

$$R = \frac{V}{I} \quad (6)$$

Then

$$\rho = \frac{\pi e}{\text{Ln}2} \cdot \frac{V}{I} \quad (7)$$

The obtained values are shown on Table-1.

TABLE-1
VALUES OF 27 MEASURE POINTS

Tablet	Value N°: 1 (Ω^* cm)	Value N°: 2 (Ω^* cm)	Value N°: 3 (Ω^* cm)	Average (Ω^* cm)
3H	0.9642	0.95100	1.0000	0.97173
3M	0.8010	0.77140	0.9224	0.83160
3B	0.8195	1.00000	0.8971	0.90553
4H	0.9036	0.97470	0.9833	0.95387
4M	0.8753	0.94646	0.9657	0.92915
4B	0.6425	0.67480	0.6906	0.66930
6H	0.8204	0.81270	0.7960	0.80970
6M	0.8960	1.00000	0.9308	0.94227
6B	1.0400	1.16000	1.0300	1.07667
Average of the measure averages				0.89887
Variance				0.01200
Standard deviation				0.10953

The samples thickness is $e = 300 \mu\text{m}$. The obtained average value worth: $\rho = 0.89 \pm 0.012 \Omega \text{ cm}$. Present material has a conductivity of $\sigma = 1.12 \Omega^{-1} \text{ cm}^{-1}$. The realized measure does not present a dispersion considering the value of the standard deviation.

This value is acceptable since it is located in the standard interval of silicon-polycrystalline resistivity. Meanwhile the quantum theories underline that the presence of defects will disturb the periodicity of crystalline network and as a result will limit the electrons mobility. This means that electric conductivity goes decreasing there is significant concentrations of impurities.

The obtained value of $1.2 \Omega^{-1} \text{ cm}^{-1}$ reveals that a positive deviation in relation to the value of $0.35 \Omega^{-1} \text{ cm}^{-1}$, which shows the presence of vacancies.

The analysis of carbon by FTIR gave the results (Table-2). It is noted that reproducibility and an acceptable dispersion of carbon grades values. The average rate is 11 ppm. The high degree of carbon super saturation and the presence of interstitial oxygen (O_i) enhance the formation of carbon precipitates¹⁸.

TABLE-2
CARBON GRADES BY FTIR

Tablet	Carbon rate ($\times 10^{17}$ atomes/cm ³)	Carbon rate (ppm)
3H	11.06	11.060
3M	10.34	10.340
3B	11.24	11.240
4H	10.67	10.670
4M	11.12	11.120
4B	11.23	11.230
6H	11.11	11.110
6M	11.01	11.010
6B	11.46	11.460
Average:		11.026
Variance:		0.107
Standard deviation:		0.327

The traces of these impurities can also be detected by spectroscopic methods such as mass spectroscopy (ICPMS) or the graphite furnace atomic absorption spectroscopy (GF-AAS).

The spectroscopic techniques can reach a detection limits about 10^{10} atm/cm². The analyses achieved by ICP give us a variation coefficient (% RSD) included between 8 and 12 % which is unacceptable in atomic emission. This result reveals that considering the concentration level, it is hard to detect the impurities by this method. This is probably due to the reason that the used argon is not pure. The used standard does not respond to present matrix, consequently, the apparent concentrations and not actual values was found.

However, the standard solutions stream is unknown suggesting that copper concentration into solution is less than 1 ppm. It was then decided to proceed by another strategy by two stages; first, detect the elements by mass spectroscopy of secondary ions (SIMS), then analyze the traces by neutron activation.

The technique sensitivity (SIMS) seriously varies from one element to another and depends on the substrate and the effects of matrix. Basically, a few hundreds of atoms are sufficient to enable the detection of an element. Though it has to be present in the extreme surface (10 Å). The limit of detection is about 1 to 10 ppm in the first atomic or molecular layer.

The mass spectrum gives the intensity (a number of the detected secondary ions) *versus* their indicated mass by the charge mass ratio (m/z). Silicon corresponds to a mixture of three isotopes ^{28}Si , ^{29}Si and ^{30}Si . These elements clearly appear on the spectrum (Fig. 4).

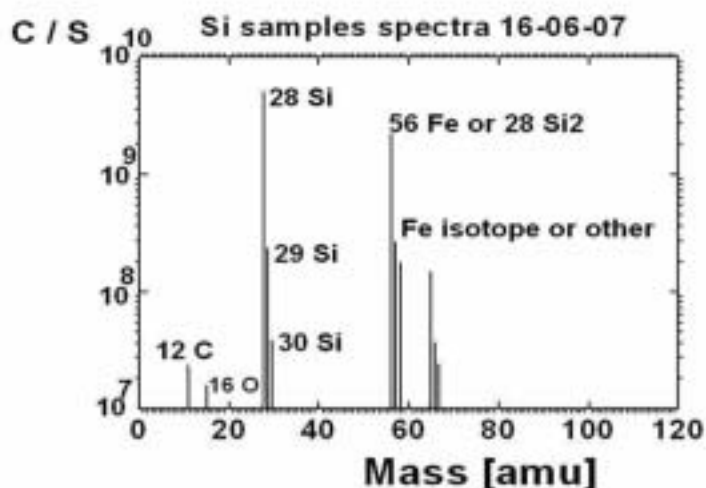


Fig. 4. The mass spectrum

The presence of iron (atomic mass 55.8) and the one of nickel (atomic mass 58.71) has been noticed. Another possible mechanism for the enhanced carbon precipitation is that co-aggregation of carbon and oxygen, as observed by previous authors²⁶, give rise to larger precipitates, which can further result in a higher precipitation rate.

Concerning the analysis by neutron activation, the choice of detection process depends on the nature of the transmitter and the complexity of the emitted spectrum.

The most powerful solution consists in recording the spectrum γ that accompanies the majority by the emissions β of the radionuclide present in the samples after activation. Unlike the spectrum β continuous in energy, which does not allow to recognize the element in case of mixture, the spectrum γ is measured hence, easier to identify. The spectrum obtained is presented in Fig. 5.

The number of radioactive atoms N^* which accumulate in the sample during the irradiation tends towards a limit: at each instant the increase in the cores number N^* is equal to the difference between the speed of formation, considered as constant (the number of target cores N being very high) and the one of decomposition

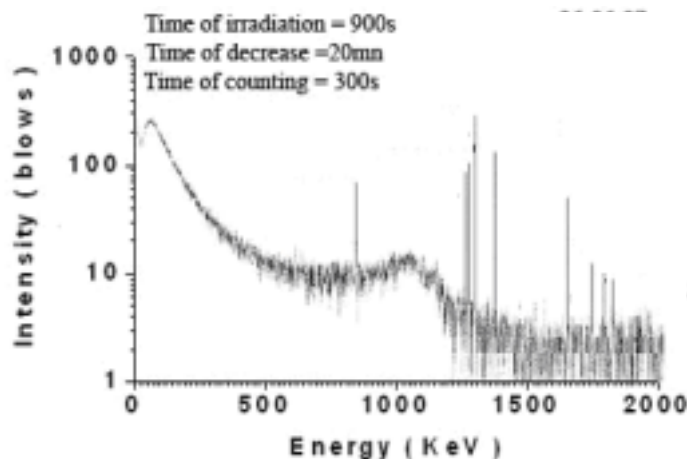


Fig. 5. The neutron activation spectrum

$$\frac{dN^*}{dt} = \varphi \sigma N - \lambda N^* \quad (8)$$

φ represent the flux of neutrons, λ the decrement radioactive constant and σ the effective section of each atom targets which the number is N .

The eqn. 8 can be written:

$$\frac{dN^*}{\lambda \cdot dt} = \frac{\varphi \sigma N}{\lambda} - N^* \quad (9)$$

The eqn. 9 is then written:

$$\frac{du}{\lambda dt} = -u \quad (10)$$

We make a change of variable $u = A - N^*$ where $A = \frac{\varphi \sigma N}{\lambda}$

The resolution gives the number of atoms N^* present at time t

It is found:

$$N^* = \frac{\varphi \sigma N}{\lambda} (1 - e^{-\lambda t}) \quad (11)$$

The results of recent neutron activation analysis studies to determine the total metal content in polycrystalline (mc)-Si materials. The results of counting are given in Table-3.

The calculation parameters are: 80 mg masses, the energetic profile of incidental flux is constituted of fast neutrons. ($\Phi_R = 3.10^{12} \text{ n cm}^{-2} \text{ s}^{-1}$; $E = 2 \text{ Mev}$), thermal neutrons ($\Phi_{th} = 10^{13} \text{ n cm}^{-2} \text{ s}^{-1}$; $E = 0.025 \text{ ev}$) and epithermal neutrons ($\Phi_{epi} = 7.1011 \text{ n cm}^{-2} \text{ s}^{-1}$; $E > 4.9 \text{ ev}$), irradiation time 15 mn, after 20 mn of decrement, acquisitions of 300 s are carried out, the results are given according to the statistical criterion of curie (Bq/g of matter).

TABLE-3
RESULTS OF IMPURITIES COUNTING (Ti, Cu AND Ni)

Sample	Ti (Bq/g)	Cu (Bq/g)	Ni (Bq/g)
3H	384.40	4670	1380
3M	486.08	8980	2590
3B	401.45	7300	1470
4H	369.24	7320	1870
4M	389.30	5410	1490
4B	387.38	4520	1500
6H	381.07	5960	1420
6M	444.86	7610	1580
6B	463.74	7900	1970

For the analyzed elements, the concentrations found are included between two level values 10 and 100 ppb. This interval corresponds to the measured activity (expressed by disintegration per second) which does not exceed the 9000, 500 and 2600 Bq, respectively for copper, titanium and nickel.

The mass of the bombarded sample is 0.08 g which represents a variability of impurities measure of $8 \cdot 10^{-10}$ g at $8 \cdot 10^{-9}$ g. In order to exploit these values, we will convert these masses into concentration expressed in atom/cm³. Measures were made on a sample of 80 mg = 0.08 g, thus a volume of $0.08 \text{ g} / 2.03 \text{ cm}^3 = 0.0394 \text{ cm}^3$. After calculations the concentrations are given in Table-4.

TABLE-4
IMPURITIES CONCENTRATIONS

Element	Atomic Mass (g)	Concentration (at/cm ³)
Ti	47.90	$2.50 \cdot 10^{14}$ – $2.5 \cdot 10^{13}$
Cu	63.54	$1.20 \cdot 10^{15}$ – $1.2 \cdot 10^{14}$
Ni	58.71	$2.08 \cdot 10^{15}$ – $2.0 \cdot 10^{14}$

It is observed that the impurities concentration in the medium are higher. The impurities in the bottom of the ingots originate from the crucible. The impurities in the top originate from impurities dissolved in the liquid silicon, which have segregated to the top layer of the ingot and after solidification diffuse. These results practically agree with those given by Revel²⁵ (Table-5).

TABLE-5
STANDARD CONCENTRATIONS OF THE Fe, Ti, Ni, Cu, C AND O IMPURITIES

Element	Raw material Eg-Si (at/cm ³)	Ingot (at/cm ³)
Iron	$< 1 \cdot 10^{14}$	$1 \cdot 10^{13}$
Nickel	$< 7 \cdot 10^{13}$	$< 3 \cdot 10^{14}$
Titanium	$< 1 \cdot 10^{15}$	$< 2 \cdot 10^{15}$
Copper	$< 4 \cdot 10^{12}$	$1 \cdot 10^{13}$
Carbon	-	$4-14 \cdot 10^{17}$
Oxygen	-	$6-12 \cdot 10^{17}$

Fig. 6 represent the distribution of impurities in the ingot respectively for Ti, Ni and Cu.

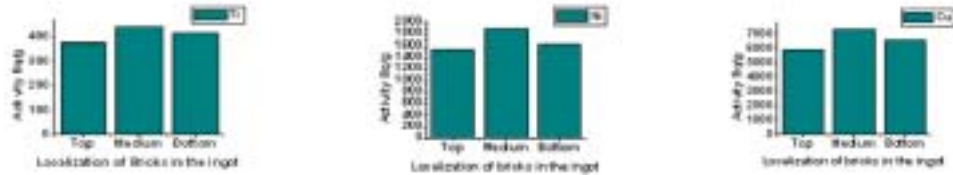


Fig. 6. Distribution of titanium, nickel and copper grades in ingot

To determine the dislocation density, an optical microscope was used and nine micrographics were taken.

The emergence points of dislocations are the black stains (sometimes transparent) almost circular (at times aligned)²³. Fig. 7 shows micrographics with a 300 μm size zone for an enlargement of G500. One can claim that the average value is equal to $6.16 \cdot 10^5$ points of emergence/cm². This value seems appreciable to us, in general concentration does not exceed $10^5/\text{cm}^2$. Several factors can contribute to increase this value. Dislocations are naturally present in crystalline materials, their growth condition leaves an imperfect structure. When the molten metal cools in a crucible, it can cling in it. The different contractions of the metal and the crucible generates constraints with the interface, sufficiently to produce dislocations.

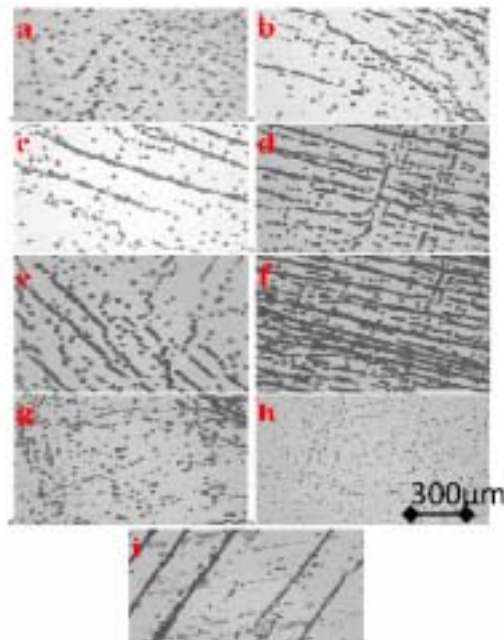


Fig. 7a-i. Images of the emergence points of dislocations (G500) in various samples for zones of the squares (1 to 9)

The Table-6 gives the results of counting.

TABLE-6
COUNTING RESULTS

Square zone	Amount of emergence points in the zone	Amount of emergence points/cm ²
1	225	248890
2	360	400000
3	355	394444
4	748	831111
5	424	471111
6	1329	1476667
7	653	725555
8	527	585555
9	373	414444
Average	555	616420

They result from the gathering of a great number of vacancies during the crystal cooling. They agglomerate in buckles extending toward the traction direction by addition of new vacancies. Impurities could precipitates in the molten metal during cooling, because of the dilatation coefficients that varies between the precipitate and the metal surrounding it. There can be generation of stresses and birth of dislocations. The Dislocations can appear by tapes of slipping due to a plastic deformation.

X-rays diffraction shows that we have only one phase of silicon (Fig. 8).

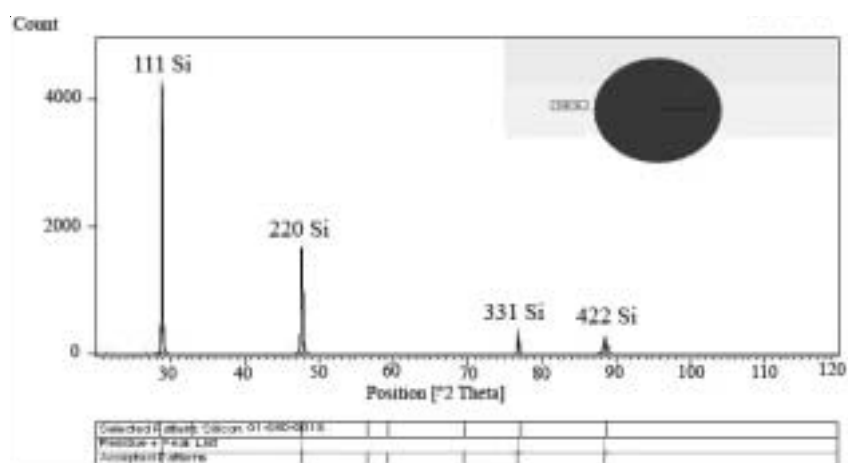


Fig. 8. Main graphics of silicon specimen

Fig. 9 gives the plot of identified phases, it corresponds clearly to a silicon phase.

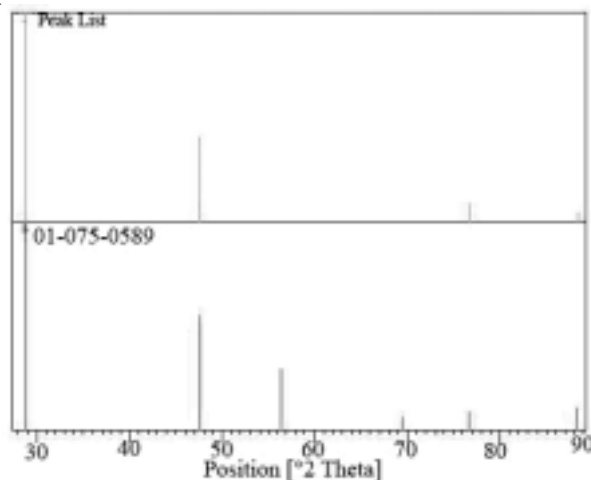


Fig. 9. Plot of identified phases of silicon specimen

The Crystallographic parameters are given in Table-7.

TABLE-7
CRYSTALLOGRAPHIC PARAMETERS

Mineral name	Silicon, syn
Chemical formula	Si
Crystal system	Cubic
Space group	Fd-3m
Space group number	227
a (Å) = b (Å) = c (Å)	5,4307
α (°) = β (°) = γ (°)	90.00
Calculated density (g/cm ³)	2.33
Measured density (g/cm ³)	2.23
Z	8.00
RIR	4.55
Volume of cell (10 ⁶ pm ³)	160.17

Conclusion

In this study we have determined the concentration of some impurities such as carbon, iron, copper, titanium, nickel as well as some properties of the flat product (polycrystalline silicon) such as thickness, resistance, rigidity, roughness and flatness. We have also estimated the dislocations densities. The analysis of results given by inductive sensor displays an average value of the thickness of the tablets which is $300 \pm 10 \mu\text{m}$ and the average value of Young's module is 17.71Gpa. The maximum value of roughness does not exceed $5.25 \mu\text{m}$. The obtained value of $1.2 \Omega^{-1} \text{cm}^{-1}$ reveals that a positive deviation is observed in relation to the value of $0.35 \Omega^{-1} \text{cm}^{-1}$. This point up the presence of vacancies.

A reproducibility and an acceptable dispersion of carbon grades values is also noticed. The average rate is 11 ppm; one can claim that the average value is equal to 6.16 10⁵ points of emergence/cm². This value seems appreciable, in general concentration does not exceed 10⁵/cm². It is estimated that several factors can contribute to increase this value. The results of neutron activation analysis show that the concentrations of the analyzed elements are included between two level values 10 and 100 ppb in present polycrystalline materials. The mass spectrum obtained by SIMS shows a mixture of three isotopes ²⁸Si, ²⁹Si and ³⁰Si. X-rays diffraction shows that we have only one phase of silicon.

REFERENCES

1. R. Bernard, M. Menguy and R. Schwartz, *The Solar Radiation Conversion and Application, Technique and Documentation*, Lavoisier, Paris (1980).
2. J.M. Gee, R.R. King and K.W. Mitchell, *Proceeding of the 25th IEEE Photovoltaic Specialists Conference*, Washington DC, p. 409 (1996).
3. A. Rohatgi and S. Narasimha, *Solar Energy Materials and Solar Cells*, **48**, 87 (1997).
4. S.A. McHugo, H. Hieslmair and E.R. Weber, *Appl. Phys. A*, **64**, 127 (1997).
5. A. Mesli and T. Heiser, *Defect Diffusion Forum*, **89**, 131 (1996).
6. S.A. McHugo, A. Mohammed, A.C. Thompson, B. Lai and Z. Cai, *J. Appl. Phys.*, **91**, 6396 (2002).
7. C. Cabanel and J.Y. Laval, *J. Appl. Phys.*, **67**, 1425 (1990).
8. T.S. Fell, P.R. Wilshaw and M.D.D. Coteau, *Phys. Stat. Sol. (A)*, **138**, 695 (1993).
9. S.A. McHugo, *Appl. Phys. Lett.*, **71**, 1984 (1997).
10. L.J. Geerligs : mc-Si: L.J. Geerligs, "Mc-Si: Relation Between Ingot Quality and Cell Efficiency", Proc. 12th Workshop on Crystalline Silicon Solar Materials and Processes", NREL/BK-520-32717, August 2002.
11. F. Shimura, *J. Appl. Phys.*, **59**, 3251 (1986).
12. Q. Sun, K.H. Yao, J. Lagowski and H.C. Gatos, *J. Appl. Phys.*, **67**, 4313 (1990).
13. S. Hahn, M. Arst, K.N. Ritz, S. Shatas, H.J. Stein, Z.U. Rek and W.A. Tiller, *J. Appl. Phys.*, **64**, 849 (1988).
14. P. Liu, X. Ma, J. Zhang, L. Li and D. Que, *J. Appl. Phys.*, **87**, 3669 (2000).
15. J.-Y. Huh, U. Giisele and T.Y. Tan, *J. Appl. Phys.*, **78**, 5926 (1995).
16. M.S. Carroll, C.-L. Chang, J.C. Sturm and T. Buyuklimanli, *Appl. Phys. Lett.*, **73**, 3695 (1998).
17. P.A. Stolk, D.J. Eaglesham, H.-J. Gossmann and J.M. Poate, *Appl. Phys. Lett.*, **66**, 1370 (1995).
18. J. Lu, G. Rozgonyi, J. Rand and R. Jonczyk, *J. Crystal Growth*, **269**, 599 (2004)
19. J.H. Bungey, *Testing of Concrete in Structures*, Surrey University Press, ISBN 0-903384-61-2. London, edn. 2 (1989).
20. L.B. Valdes, *Proc. I.R.E.*, **42**, 420 (1954).
21. F.M. Smith, *Bell System Technical J.*, **37**, 711 (1958).
22. H. Rauh, *Waker's Atlas for Characterization of Defect in Silicon*, pp. 5-9.
23. D. Shimmel, *J. Electrochem. Soc.*, **126**, 479 (1979).
24. B. Equer, *Energie Solaire Photovoltaïque, Physique et technologie de la conversion photovoltaïque*. Ellipses Editions Marqueting, Vol. 1 (1993).
25. G. Revel, N. Deschamps, C. Dardenne, J.L. Pastol, D. Hania and J.L. Nguyen Dinh, *Radional. Nucl. Chem. Lett.*, **85**, 137 (1984).
26. F. Shimura, R.S. Hockett, D.A. Reed and D.H. Wayne, *Appl. Phys. Lett.*, **47**, 794 (1985).